Electronic Supplementary Information

Singlet Exciton and Singlet/Triplet Self-Trapped Excitons for Ultra-Broadband White-Light Emission in a Zero-Dimensional Cadmium Bromide Hybrid †

Huizhi Gao,[a] Zhuoya Lu,[a] Xingxing Zhao,[a] Ke Zhang,[a] Xudong Zhu,[b,c] Rixin Cheng,[a] Shi-Li Li,[a] Zhikai Qi,[a,*] and Xian-Ming Zhang [a,d,*]

[a] *Key Laboratory of Magnetic Molecules & Magnetic Information Materials (Ministry of Education), School of Chemistry & Material Science, Shanxi Normal University, Taiyuan 030032 P. R. China.*
[b] *CAS Key Laboratory of Quantum Information, University of Science and Technology of China, Hefei, Anhui, 230026, China*
[c] *Institute of Artificial Intelligence, Hefei Comprehensive National Science Center, Hefei, Anhui, 230026, China*
[d] *Key Laboratory of Interface Science and Engineering in Advanced Material (Ministry of Education), College of Chemistry and Chemical Engineering, Taiyuan University of Technology, Taiyuan 030024, P. R. China.*

**Email: qizk@sxnu.edu.cn (Z. Q.); zhangxm@sxnu.edu.cn (X.-M. Z.)*

Contents

1. Methods

1.1 Hirshfeld surface analysis. Hirshfeld surfaces and the related two-dimensional (2D) fingerprint plots of $(H_2AMP)^{2+}$ cations in asymmetric unit were calculated by using the *CrystalExplorer* 21.5 program with inputting structure file in CIF format. In this work, all the Hirshfeld surfaces were generated using a standard (high) surface resolution. The three-dimensional (3D) Hirshfeld surfaces and 2D fingerprint plots are unique for any crystal structure. The intensity of intermolecular interaction is mapped onto the Hirshfeld surface by using the respective red-blue-white scheme: where the white or green regions exactly correspond to the distance of Van der Waals contact, the blue regions correspond to longer contacts, and the red regions represent closer contacts. In 2D fingerprint plots, each point represents an individual pair (d_i, d_e), reflecting the distances to the nearest atom inside (d_i) and outside (d_e) of the Hirshfeld surface, and the frequency of occurrence for these points corresponds to the color from blue (low), through green, to red (highest). The normalized contact distance d_{norm} is based on d_e, d_i, and the van der Waals (vdW) radii of the two atoms external (r_e^{vdW}) and internal (r_i^{vdW}) to the surface:

$$d_{norm} = \frac{d_i - r^{vdW}}{r_i^{vdW}} + \frac{d_e - r}{r_e^{vdW}}$$

d_{norm} surface is used for the identification of very close intermolecular interactions. The value of d_{norm} is negative or positive when intermolecular r contacts are shorter or longer than r^{vdW}, respectively.

1.2 Fabrication of device. Crystal samples of **1** (200 mg) were fully ground into powder and uniformly mixed with modified acrylic adhesive (200 mg). The obtained mixture of **1** was then carefully coated onto a commercial ultraviolet LED lamp with an emission wavelength of 360−365 nm and a working voltage of 3 V. Subsequently, the fabricated device was placed in air for about 2 h to evaporate the solvent and further dried in a vacuum oven at 333 K for 12 h to remove the residual solvent.

1.3 Density Functional Theory Calculations. First-principles calculations were performed by density-functional theory using Vienna ab-initio simulation package (VASP, version 5.4), in which all-electron information was reconstructed by projected augmented-wave (PAW) pseudopotentials. The exchange-correlation energy was treated by the Perdew-Burke-Ernzerhof (PBE) exchange-correlation functional in the scheme of generalized gradient approximation. The kinetic energy cutoff for all cases was determined to be 520 eV. The convergence thresholds for the electronic calculations and ionic relaxations were chosen as 10^{-6} eV and 0.01 eV/Å, respectively. The standard Monkhorst-Pack *k*-point grids with density of 0.1 $Å^{-1}$ were used for Brillouin zone sampling. The valence electron configurations applied in this work were treated as Cd ($5s^2 4p^6$), C ($2s^2 2p^2$), Br ($4s^2 4p^5$), N ($2s^2 2p^3$), and H ($1s^1$). The highest occupied molecular orbitals (HOMO), as well as lowest unoccupied molecular orbitals (LUMO) for 0D Cd-based halide hybrid in this work, were also carried out by DFT calculations with orbital occupancies.

2. Supporting figures

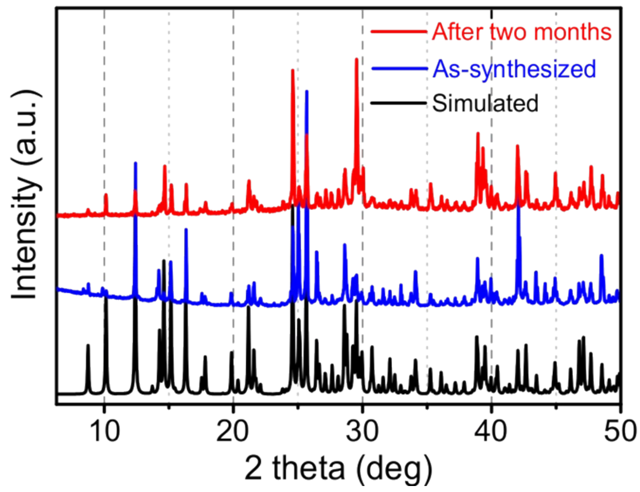

Fig. S1 Experimental and simulated powder XRD data of $(H_2AMP)CdBr_4{\cdot}H_2O$.

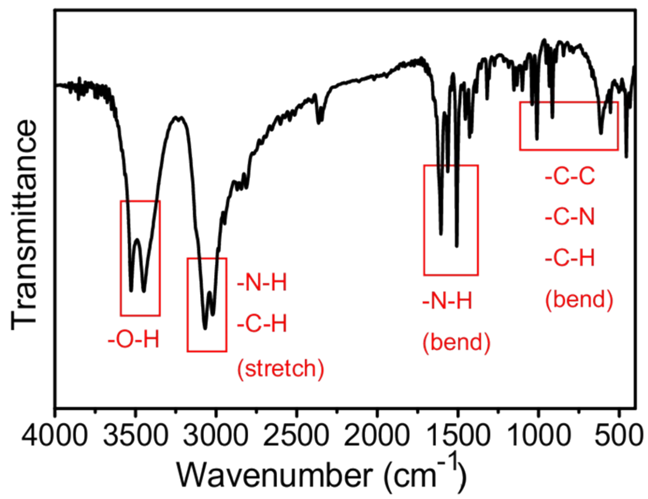

Fig. S2 FT - IR spectrum of $(H_2AMP)CdBr_4{\cdot}H_2O$.

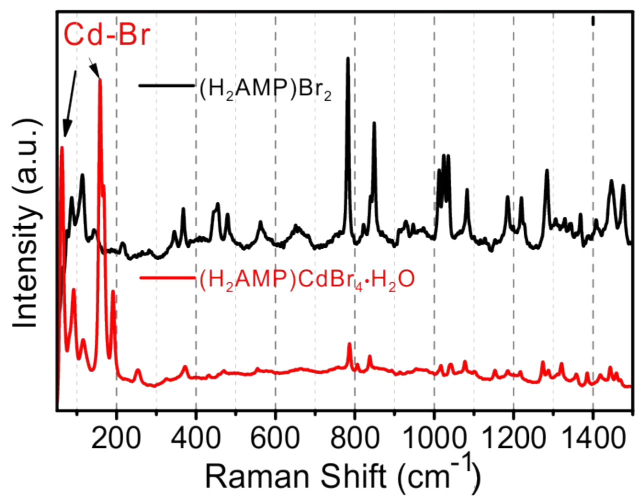

Fig. S3 Raman spectra of $(H_2AMP)Br_2$ and $(H_2AMP)CdBr_4{\cdot}H_2O$.

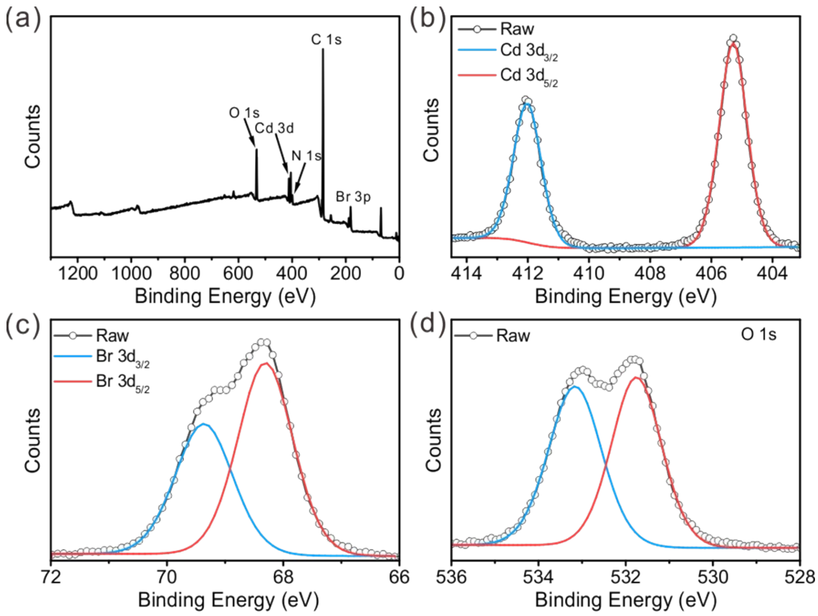

Fig. S4 (a) Whole XPS survey spectra of $(H_2AMP)CdBr_4{\cdot}H_2O$. High-resolution scan of (b) Cd 3d, (c) Br 3d, and (d) O 1s electrons.

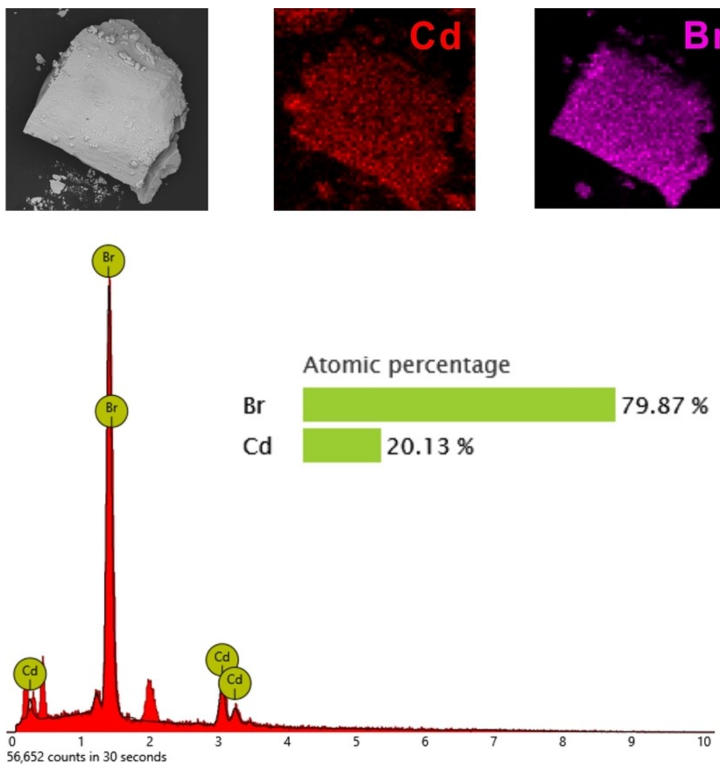

Fig. S5 EDS for elemental mapping of crystal sample of $(H_2AMP)CdBr_4{\cdot}H_2O$.

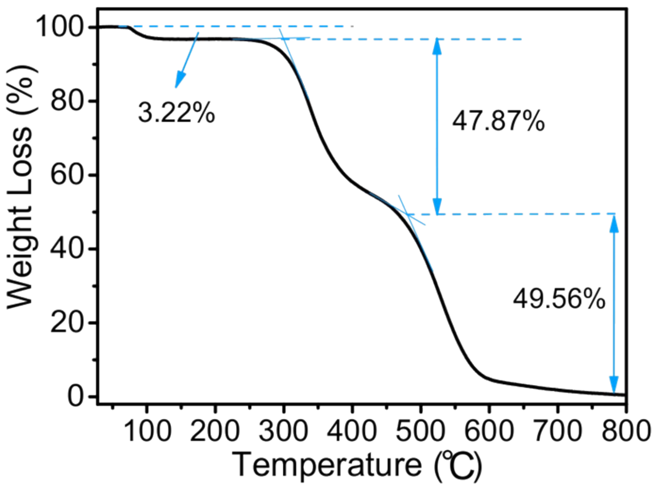

Fig. S6 Thermogravimetric curve of $(H_2AMP)CdBr_4{\cdot}H_2O$.

The TGA curve of $(H_2AMP)CdBr_4{\cdot}H_2O$ exhibits three weight loss steps in the temperature range from 72 to 800℃. The weight loss of about 3.22% at 72℃ corresponds to the escape of H_2O molecular in $(H_2AMP)CdBr_4{\cdot}H_2O$ (calcd. 3.19%). With the increasing temperature, the weight loss in the second and third steps is almost continuous. The second weight loss of 47.87% in 106–299°C was attributed to the elimination of organic cations $(H_2AMP)^{2+}$ and two Br^- of $[CdBr_4]^{2-}$ (calcd. 48.64%), and the third weight loss is about 49.56% assigned to the removal of the residual component in inorganic $[CdBr_4]^{2-}$ blocks (calcd. 48.18%).

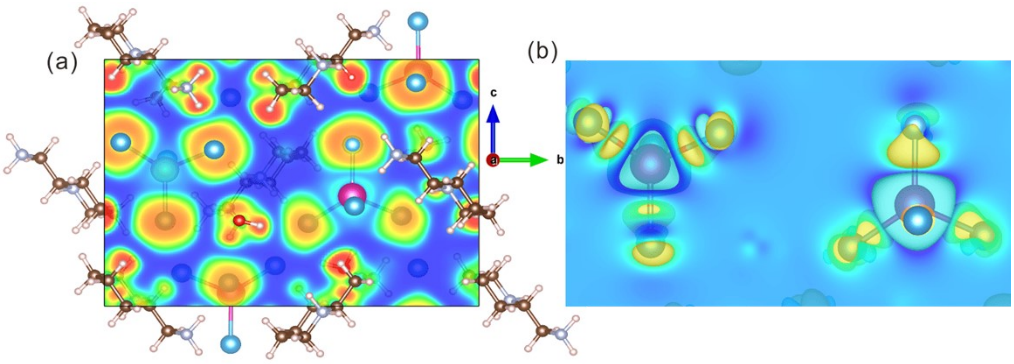

Fig. S7 2D maps of (a) electron localization function (ELF) and (b) electron differential density (EDD) for $(H_2AMP)CdBr_4{\cdot}H_2O$.

Details: Electron localization function (ELF) was introduced in terms of the probability of electron pairs with the same spin. The topology of the ELF can be used to define basins within which one or more electron pairs (of different spin) are to be found. Gradient paths end within each subsystem at what are called attractors, which correspond to cores, lone pairs, and electrons localized to bonds. The number of atomic valence shells in which a valence basin participates is the synaptic order of the valence basins. Lone pairs and bonds involving hydrogen atoms are associated with monosynaptic basins, whereas covalent and polar bonds usually exhibit disynaptic basins. The electron population and shape of the ELF basins are commonly used to distinguish bond interactions. As the volume was determined by the ELF isosurfaces, the localization domain was introduced to define a hierarchy of the localization basins based on the ELF value for the isosurfaces. The electron differential density (EDD) map of $(H_2AMP)CdBr_4{\cdot}H_2O$ is defined as ρdiff = $\rho_{AB} - \rho_A - \rho_B$, where ρ_{AB} denotes the electron density of all atoms in the unit cell, while ρ_B and ρ_A represent the charge densities of the isolated Cd and other atoms except Cd, respectively. EDD map was generated by using VESTA software package.

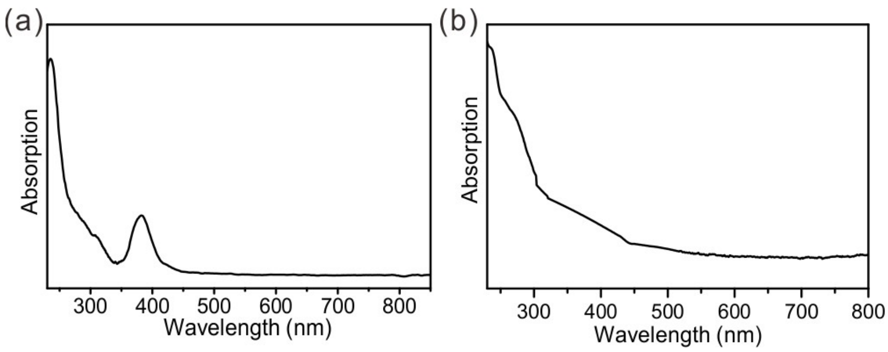

Fig. S8 UV-vis absorption spectrum of (a) $(H_2AMP)CdBr_4{\cdot}H_2O$ and (b) $(H_2AMP)Br_2$. By comparing the absorption spectra of hybrid and organic salt, the absorption peak at < 338 nm can be assigned to the organic molecules.

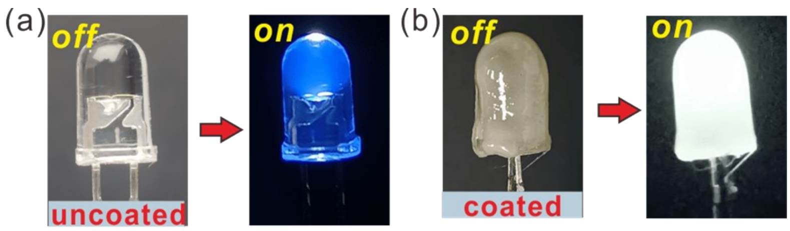

Fig. S9 (a) Photographs of ultraviolet LED lamps and (b) LED coated with a thin layer of $(H_2AMP)CdBr_4{\cdot}H_2O$ in the off and on states.

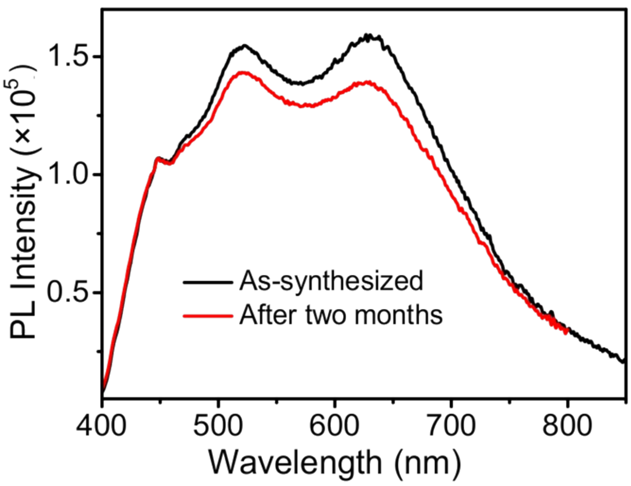

Fig. S10. Emission spectra of $(H_2AMP)CdBr_4{\cdot}H_2O$ before (black line) and after (red line) about two months.

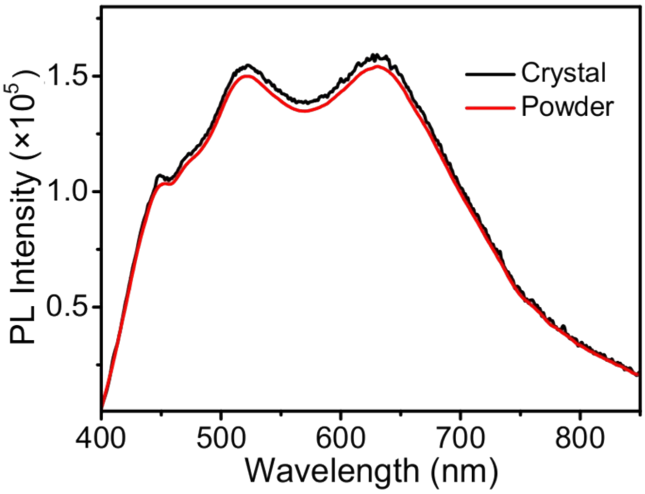

Fig. S11 Emission spectra of $(H_2AMP)CdBr_4{\cdot}H_2O$ for mm-sized bulk crystals and powder sample.

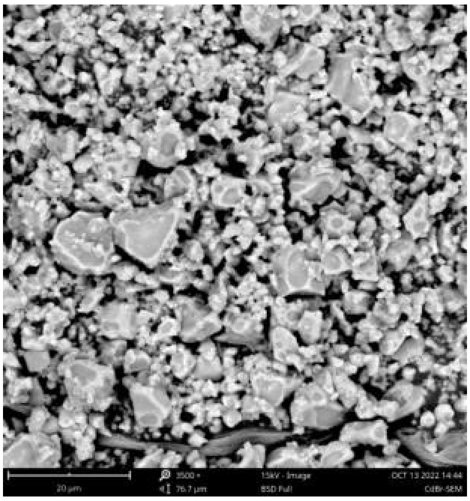

Fig. S12 SEM image of powder sample of $(H_2AMP)CdBr_4{\cdot}H_2O$.

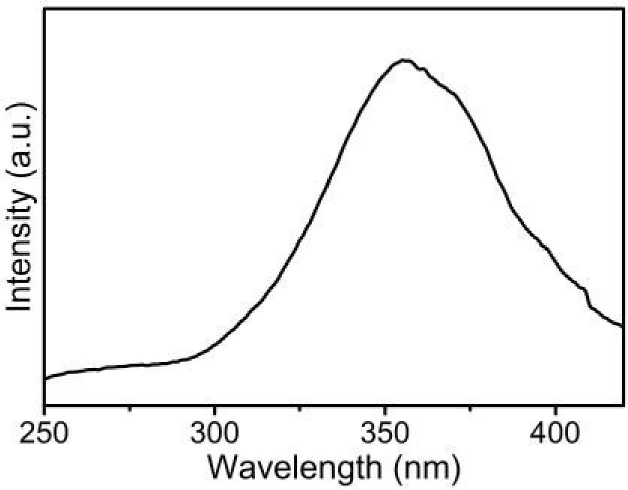

Fig. S13 Excitation spectrum of $(H_2AMP)Br_2$.

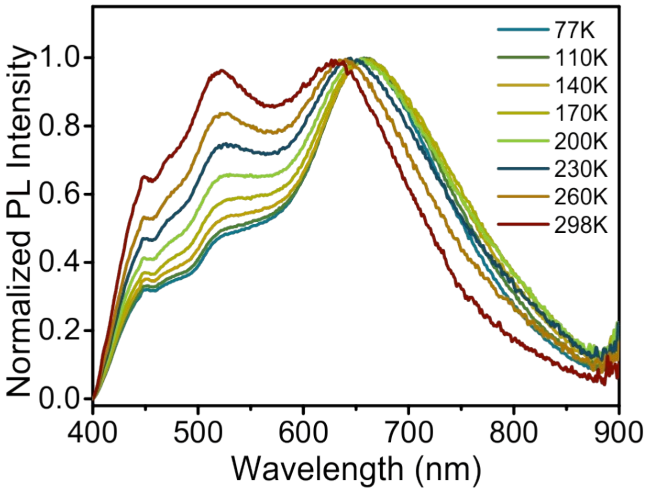

Fig. S14 Normalized temperature-dependent steady state PL spectra of $(H_2AMP)CdBr_4{\cdot}H_2O$.

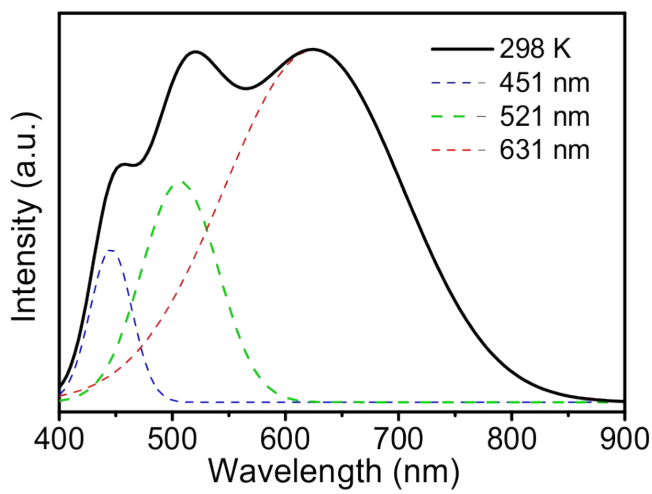

Fig. S15 Emission spectra of $(H_2AMP)CdBr_4{\cdot}H_2O$ via Gaussian fitting.

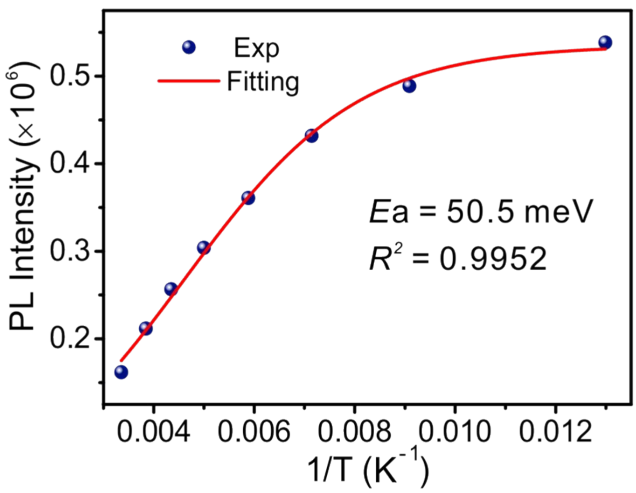

Fig. S16 PL intensity of the STE emission at 521 nm as a function of 1/T in the range of 80−300 K, where the red line shows the fitting data according to the Arrhenius equation.

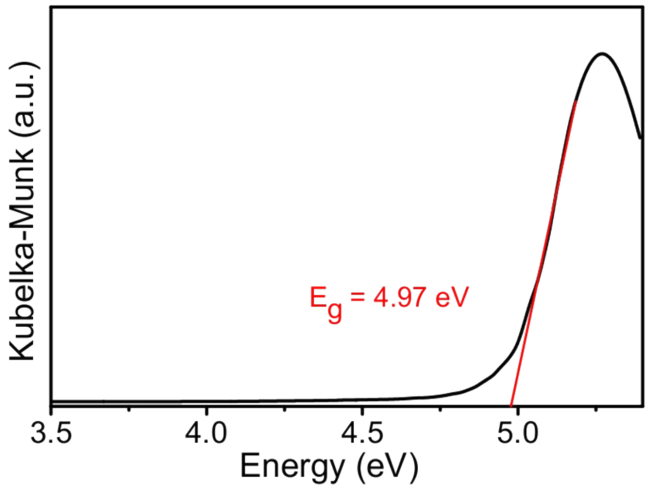

Fig. S17 UV-vis diffuse reflectance spectrum of $(H_2AMP)CdBr_4{\cdot}H_2O$.

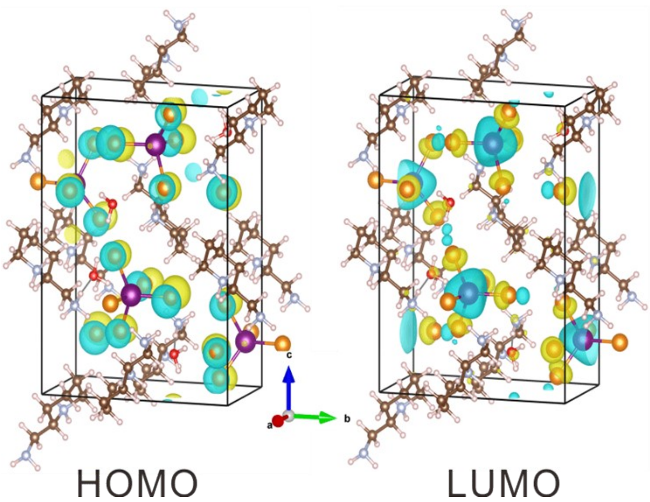

Fig. S18 HOMO and LUMO of $(H_2AMP)CdBr_4{\cdot}H_2O$.

3. Supporting tables

Table S1. Crystal data of **1**.

Compound	**1**
Formula	$C_6H_{18}Br_4CdN_2O$
Mr	566.26
T/K	293(2)
Crystal system	orthorhombic
Space group	$P2_12_12_1$
Z	4
a/Å	6.93942(13)
b/Å	12.3939(2)
c/Å	17.4403(3)
α/°	90
β/°	90
γ/°	90
V/Å^3	1499.98(5)
ρ_{calc}g/cm^3	2.508
μ/mm^{-1}	23.974
F(000)	1056
Size/mm^3	0.5×0.3×0.2
T_{max}/T_{min}	1.000/0.137
S	1.046
R_{int}/R_{sigma}	0.0735/0.0587
Reflections	9472/2915
Data/Para.	2915/132
R_1[a], wR_2[b][I>2σ(I)]	0.0531/0.1429
R_1[a], wR_2[b](all data)	0.0545/0.1452
$\Delta\rho_{max}/\Delta\rho_{min}$ / e Å^{-3}	1.32/-1.36
CCDC No.	2222028

[a]$R_1 = \sum||F_o|-|F_c||/\sum|F_o|$. [b]$wR_2 = [w(F_o^2-F_c^2)^2/w(F_o^2)^2]^{1/2}$

Table S2. Intermolecular A-H···Br/O (A = O, N) in $(H_2AMP)CdBr_4{\cdot}H_2O$.

D–H···A	d(D–H) / Å	d(H–A) / Å	d(D–A) / Å	D–H–A / °
N1–H1···Br1a	0.89	2.58	3.384(10)	151.2
N1–H1b···Br2b	0.89	2.53	3.399(10)	165.4
N2–H2c···O1	0.89	1.96	2.811(16)	159.5
N2–H2d···Br3a	0.89	2.58	3.379(12)	150.3
N2–H2e···Br1	0.89	2.54	3.416(10)	170.5
O1–H1c··Br3c	0.85	2.69	3.332(10)	133.9
O1–H1d···Br4d	0.85	2.70	3.474(10)	151.7

Symmetric code: (a) -1+x, +y, +z; (b) 2-x, 1/2+y, 1/2-z; (c) 5/2-x, 2-y, 1/2+z; (d) 2-x, -1/2+y, 1/2-z

Table S3. Selective bond lengths and bond angles.

Atom–Atom	Length / Å	Atom–Atom	Length / Å
Cd1–Br1	2.6276(14)	Cd1–Br4	2.5860(14)
Cd1–Br2	2.5839(16)	Cd1–Br3	2.5542(14)
Atom–Atom–Atom	**Angle / °**	**Atom–Atom–Atom**	**Angle / °**
Br2–Cd1–Br1	105.42(5)	Br3–Cd1–Br1	107.47(5)
Br2–Cd1–Br4	108.99(5)	Br3–Cd1–Br2	108.27(5)
Br4–Cd1–Br1	109.01(5)	Br3–Cd1–Br4	117.06(5)

Table S4. FWHM (> 200 nm) of reported single-component white-light emitters.

Compound	FWHM (nm)	Ref.
$[C_5H_9\text{-}NH_3]_4CdBr_6$	~350	*J. Mater. Chem. C,* **2017**, *5,* 4731
$[(C_3H_7)_4N]_2Cu_2I_4$	~300	*ACS Appl. Mater. Interfaces,* **2022**, *14,* 12395
$(H_2AMP)CdBr_4\cdot H_2O$	**285**	**Our work**
$(C_5N_2H_{14})SnCl_6$	254	*Adv. Optical Mater.,* **2021**, 2002246
$(TMEDA)_5Sb_6Cl_{28}\cdot 2H_2O$	253	*J. Mater. Chem. C,* **2021**, *9,* 15942–15948
$(TAE)_2[Pb_2Cl_{10}](Cl)_2$	247	*ACS Photonics,* **2020**, *7,* 1178−1187
$(C_6H_7NBr)_2CdBr_4$	244	*Mater. Chem. Front.,* **2023**, *7,* 705–712
$(C_6H_7NCl)_2CdCl_4$	218	*Mater. Chem. Front.,* **2023**, *7,* 705–712
$(C_6H_8N)_6InBr_9$	~238	*J. Mater. Chem. C,* **2022**, *10,* 1999
$(C_5H_7N_2)_2HgBr_4\cdot H_2O$	233	*Chem. Mater.,* **2019**, *31,* 2983–2991
$(EDBE)[PbBr_4]$	215	*J. Am. Chem. Soc.,* **2014**, *136,* 13154–13157
$(EDBE)[PbCl_4]$	208	*J. Am. Chem. Soc.,* **2014**, *136,* 13154–13157
$(C_6H_7ClN)CdCl_3$	213	*Inorg. Chem.,* **2022**, *61,* 4752−4759
$C_4N_2H_{14}PbBr_4$	~210	*Nat. Commun.,* **2017**, *8,* 14051
$(CH_3NH_3)_2CdCl_4$	208	*Inorg. Chem.,* **2017**, *56,* 13878–13888
$(C_3N_3H_{11}O)_2PbBr_6\cdot 4H_2O$	200	*Nat. Commun.,* **2019**, *10,* 5190
$(2cepiH)CdCl_3$	~ 200	*J. Mater. Chem. C,* **2021**, *9,* 88-94